



ELSEVIER

Ocean Modelling 3 (2001) 1–20

---

---

**Ocean  
Modelling**

---

---

www.elsevier.com/locate/omodo1

# Open boundary conditions for long-term integration of regional oceanic models

Patrick Marchesiello<sup>\*</sup>, James C. McWilliams, Alexander Shchepetkin

*UCLA, Institute of Geophysics and Planetary Physics, Los Angeles, CA 90095-1567, USA*

Received 31 August 2000; received in revised form 2 November 2000; accepted 2 November 2000

---

## Abstract

Regional oceanic models can be developed and used efficiently for the investigation of regional and coastal domains, provided a satisfactory prescription for the open boundary conditions (OBCs) is found. We propose in this paper an adaptive algorithm where inward and outward information fluxes are treated separately. Because of the essentially hyperbolic nature of the incompressible, hydrostatic Primitive Equations, external data are required only for inward boundary fluxes. The outward fluxes are treated with a new algorithm for two-dimensional radiation. Special attention is given to the estimation of the radiation phase speed, essential for detecting the direction of boundary fluxes. The boundary conditions are applied and assessed on a US West Coast (USWC) configuration of the Regional Oceanic Modeling System (ROMS). Our guiding principles are that the numerical solution be stable over multiple years, reach a meaningful statistical equilibrium, and be realistic with respect to the available observational data. A sensitivity analysis suggests that the oblique radiation is robust and sufficiently accurate to detect the direction of information fluxes. The adaptive nudging adequately incorporates the external information minimizing over- and under-specification problems. In addition, a volume constraint based on global correction of normal barotropic velocities improves the overall performances of the open boundary conditions. © 2001 Elsevier Science Ltd. All rights reserved.

*Keywords:* Open boundary conditions; Modeling; Ocean circulation

---

## 1. Introduction

The ocean around coastal areas is rich in dynamical phenomena interacting on multiple scales. Coastal currents are responsive to local wind forcing, tides, and remote influences transmitted

---

<sup>\*</sup> Corresponding author. Tel.: +1-310-825-5402; fax: +1-310-206-5219.  
*E-mail address:* patrickm@atmos.ucla.edu (P. Marchesiello).

from offshore and along the coastal waveguide. They develop local jets with large topographically modulated variability. Offshore currents have intrinsic mesoscale variability from instabilities of the persistent along-shore currents. They are generated as part of the large-scale circulation or emerge from the near-shore regions. In modeling practice it is infeasible for any regular computational grid to be large enough to resolve well all types of currents, in order to examine their dynamical interactions. Instead, regional models can be used to calculate local currents under the influences of local forcing and the larger-scale circulation, provided a satisfactory prescription for the lateral boundaries is found.

Ideal, compressible fluid dynamics is a hyperbolic PDE system. Successive balance approximations are often used in oceanic modeling of currents – incompressible mass balance, hydrostatic vertical momentum balance, gradient-wind or geostrophic horizontal momentum balance, etc., – and they progressively transform the system behavior towards ellipticity for the currents with larger space and time scales. The loss of complete hyperbolicity has a potentially profound influence on the well-posedness of the initial boundary value problem. Our focus here is on the incompressible, hydrostatic Primitive Equations at a large Reynolds number. The local treatment of open boundary conditions for this system is known to be ill posed (Olinger and Sundstrom, 1978; Bennett, 1992), i.e., we cannot define a set of boundary conditions which guarantees existence of a stable, unique solution. Despite ill-posedness, when the number of boundary conditions is over-specified, the discrete approximation may well be stable, but the underlying solution being approximated is not generally continuous and the interior solution can be rapidly contaminated with error. The difficult behavior responsible for discontinuities at open boundaries is essentially hyperbolic in the sense that the local evolution is dominated by local spatial propagation of information. In this case, no physical boundary condition is required when information is directed outward, and discretized boundary conditions can be viewed as a mathematical artifact of the grid discretization. These, generally called *open boundary conditions* (OBCs), are a computational necessity with rather uncertain physical principles at their foundation. According to Roed and Cooper (1986), an open boundary should allow the perturbations generated inside the computational domain to leave it without deterioration of the inner model solution. However, there is a sometimes competing requirement that physically important external information be conveyed inwards, otherwise the system may be under-specified.

A large number of open boundary conditions have been proposed in the literature (see Palma and Matano, 1998, for a recent review). Some of them are based on a linearized version of the primitive equations, that is a *reduced physics* describing a local solution. Others are *relaxation* schemes which restore the prognostic variables to a reference state within specified regions. The most popular OBCs are derived from the *radiation* equation of Sommerfeld (1949), which can provide a simple and stable extrapolation of the interior solution, guided by the idea that interior disturbances approaching the boundary should propagate through it in a wave-like way. Here, the primary issue is the proper formulation of the wave phase speed. In special cases, it may be assumed that the dominant wave packet approaching the boundary has identifiable oceanic dynamics such as non-dispersive gravity waves (Chapman, 1985), but a more general approach was proposed by Orlanski (1976) who estimated the phase speed generically by using interior values. This latter idea also provides a natural basis for a dynamic open boundary algorithm in which inward and outward fluxes can be detected and treated separately.

The testing of open boundary conditions is generally done for isolated phenomena in the shallow water approximation. For example, in Miller and Thorpe (1981) and Chapman (1985), the solution for different OBCs is compared to a benchmark run with extended computational domain or cyclic conditions or, when possible, to an analytical solution. Because of the ill-posedness of the open boundary problem, the results of these tests are confusing and sometimes conflicting (Treguier et al., 2000; Palma and Matano, 1998), especially when the algorithms are applied to more complex and realistic three-dimensional configurations where the long-term solution is affected by large-scale forcing and boundary fluxes. In fact, rather few OBCs have been proposed for Primitive-Equation oceanic models applied to regional oceanic configurations. For such applications, testing is difficult. Our guiding principles are that we want our numerical solution to be *stable* over multiple years and reach *statistical equilibrium*. We also want the solution to be *realistic*, given the available knowledge from observations or large-domain models, though we accept that it may sometimes be difficult to distinguish the OBCs' role in unrealistic solutions.

Among studies succeeding in this approach, Stevens (1990) proposed and tested numerical schemes for the Geophysical Fluid Dynamics Laboratory (GFDL) oceanic model (having characteristics such as an Arakawa B-grid and rigid-lid approximation). The method combined radiation conditions for tracer fields and linearized momentum equations to compute velocities at boundary points. These conditions were used in the Fine Resolution Antarctic Model experiment (Stevens, 1991) and other applications. Barnier et al. (1998) proposed different physical assumptions for the S-coordinate Primitive Equation Model (SPEM: C-grid, rigid-lid), combining for each variable two-dimensional radiation techniques and relaxation to climatological data. The conditions were used to model the South Atlantic dynamical equilibrium using three open boundaries (Marchesiello et al., 1998, with SPEM; Treguier et al., 2000, with the Océan Parallélisé Model, OPA). Our attention has been brought to the dual character of lateral boundaries, consistent with the nature of hyperbolic equations. When information fluxes are directed outward, the boundary is *passive* (i.e. the boundary solution is determined by the interior solution). For inward fluxes, the boundary is *active* (i.e. the boundary solution determines the interior solution). The use of a dynamic or *adaptive* approach also is made in other regional configurations (Marchesiello and Middleton, 2000, application to the Western Tasman Sea; Penduff et al., 2000, application to the Eastern North Atlantic).

We propose here an alternative version of the OBCs implemented in the Regional Oceanic Modeling System (ROMS) (Shchepetkin and McWilliams, 2000), with significant modifications to the computational algorithm. ROMS is a free-surface, primitive-equation, curvilinear-coordinate oceanic model in which barotropic and baroclinic momentum equations are resolved separately. The model is written for multi-threaded computer architectures and features higher-order numerical schemes for space and time differencing to optimize the effective resolution of the model. We have developed compatible numerical schemes for the OBCs to achieve stable, realistic equilibrium solutions. The OBCs are applied in a US West Coast (USWC) configuration which will be briefly described in this paper. The OBCs are similarly being applied with success to model the southern Agulhas Current and Benguela System (Penven et al., 2000), and the West Coast circulation of Central America (June Chang, personal communication). Good performance is also found for more isolated phenomena in the coastal ocean (Hetland and Signell, 2000, simulating river plumes in a comparative study of ROMS and the Princeton Ocean Model, POM).

## 2. Strategy: adaptive open boundary conditions

In the 1970s, atmospheric forecast modelers, realizing the need for high-spatial resolution, began investigating regional applications. In the attempt to prescribe observed data at the boundaries of regional domains, they encountered the problem of over-specification. Over-specification occurs when external data are not compatible with the interior equations. One-way and two-way grid-nesting techniques were then devised to exchange information at the interface between fine-mesh, regional models and coarse-mesh, large-domain models. In the case of nesting, the external data are almost compatible with the interior equations, and the strain from the over-specification is eased, although additional interface treatment is needed for remaining incompatibilities mostly related to outward fluxes. A promising methodology is adaptive mesh refinement (Blayo and Debreu, 1999), in which the dynamic interface is systematically relocated where incompatibilities are low. More classical techniques with fixed grids include flux-conservation constraint, damping, and radiation methods (Miyakoda and Rosati, 1977; Perkins et al., 1997).

Radiation methods, as proposed by Orlanski (1976), work reasonably well as passive boundary conditions, allowing disturbances to propagate out of the computational domain, but different methods are needed for the active part of the problem to avoid under-specification. In an under-specified problem, the extrapolation of quantities that should be specified results in solving the wrong differential equations (Oliger and Sundstrom, 1978). In practice, the solution may well be continuous, but the model generally drifts away from the real ocean. In Ezer et al. (1992), the character of a lateral boundary, either passive or active (generally an inflow boundary), is chosen a priori by the modeler, and external data are prescribed at the active boundary. In this case, the assumption is made that inflow- and inward-propagation boundaries are equivalent. In fact, both physical modes – such as Kelvin waves, Rossby waves, and inertia–gravity waves – and computational modes may travel upstream and have important consequences at an inflow boundary if not damped. Alternatively, relaxation (or *nudging*) terms towards external data can be added to the radiation condition (Blumberg and Kantha, 1985), or imposed along a nudging layer adjacent to the boundary (Matano and Philander, 1993). However, it may be difficult to find a good compromise for the relaxation strength which guarantees that the model solution does not drift in time while avoiding over-specification problems.

We are proposing a method of combining both active and passive characteristics in an adaptive algorithm, similar in some aspects to the one-way nesting proposed by Miyakoda and Rosati (1977). The idea is to use the radiation condition to determine whether an open boundary is passive (outward propagation) or active (inward propagation). In the case where the boundary is passive, the radiation extrapolation is applied, allowing the information from the interior solution to pass through the boundary without excessive reflection. In the active-boundary case, when dynamical equations require external information, the solution can be strongly nudged towards external data without causing an over-specification problem. The external data may be provided from observed climatologies, large-domain model climatologies, or even large-domain model time-evolving solutions (in this case, the method is one-way nesting). The performance greatly depends upon the accuracy in computing the normal phase speed of the dominating waves, as we will show.

### 3. Radiation condition

#### 3.1. Equations

The wave equation used to derive the radiation condition is based upon the work of Raymond and Kuo (1984), who considered an oblique horizontal radiation with phase velocity components both normal and tangential to the boundary.

The radiation condition for a prognostic model variable  $\phi$  is

$$\frac{\partial \phi}{\partial t} + c_x \frac{\partial \phi}{\partial x} + c_y \frac{\partial \phi}{\partial y} = 0, \quad (1)$$

where  $(x, y)$  are, respectively, the normal and tangential directions to the boundary in local Cartesian coordinates. The phase speeds  $(c_x, c_y)$  are projections of the oblique radiation, calculated from the  $\phi$  field surrounding the boundary point as follows:

$$c_x = -\frac{\partial \phi}{\partial t} \frac{\partial \phi / \partial x}{(\partial \phi^2 / \partial x) + (\partial \phi^2 / \partial y^2)} \quad (2)$$

and

$$c_y = -\frac{\partial \phi}{\partial t} \frac{\partial \phi / \partial y}{(\partial \phi^2 / \partial x) + (\partial \phi^2 / \partial y)}. \quad (3)$$

Note that this radiation equation makes sense only in a discrete form since the phase speed is derived from the same equation. Also, the equation is non-linear, which is an obstacle to its mathematical analysis. As pointed out by Raymond and Kuo (1984), the real advantage of oblique versus normal radiation is in the accuracy of the computed normal phase speed  $c_x$ . In Orlanski (1976),  $c_x$  is computed only from normal derivatives. When the direction of propagation is tangential rather than normal to the boundary, the normal derivative tends to 0. Raymond and Kuo (1984) show that in this case  $c_x$  may fluctuate rapidly between infinitely large positive and negative values (in practice, when explicit time stepping is used,  $c_x$  has to be limited by the CFL ratio  $\Delta t / \Delta x$ , where  $\Delta t$  is the model time step, and  $\Delta x$  is the model space step). For this reason, the normal phase speed computed from a one-dimensional wave equation cannot accurately determine active and passive situations. A two-dimensional wave equation certainly provides a better alternative. In the following, for convenience, lateral derivatives are computed along  $\sigma$  surfaces rather than geopotential surfaces. For normal derivatives, the difference is nil since we use a zero-gradient condition for the bathymetry across lateral boundaries. For tangential derivatives, we assume that the difference is small, and we did not find evidence that the radiation skills are affected by this assumption.

#### 3.2. Computational algorithm

The radiation algorithm provides boundary values by using an extrapolation rule based on interior values in the vicinity of the open boundary and an implicit assumption that the phase speed is a slowly varying field compared to the variables from which it is computed, so that the

propagation behavior is clean in (1). Numerical stability is usually guaranteed by the *convexity* property (i.e. the extrapolated values are represented as the weighted sum of values at the previous time step on the boundary and its neighboring points with all weighting coefficients non-negative). In the case where the algorithm detects an inward phase speed ( $c_x < 0$ ), convex extrapolation becomes impossible since it would require values outside the computational grid. In this case, a different approach is needed (see Section 4.1).

In Orlanski (1976), the phase speed is computed at the previous time step and for interior values; the radiation algorithm had explicit leapfrog time differencing and upstream space differencing for normal gradients; and the phase speed is bounded to satisfy the CFL condition. Raymond and Kuo (1984) adopted the same algorithm and added a centered space-differencing scheme to compute tangential gradients. In doing so, they violated the convexity property. Among interesting variations to Orlanski (1976); Miller and Thorpe (1981) proposed a first-order, forward time differencing for simplicity and improved accuracy, which was used by Stevens (1990) in the GFDL model. Also, Chapman (1985), in a comparative study, shows best performances when the phase speed is computed at the current time.

We choose the following algorithmic features:

- Implicit time differencing for normal propagation.
- First-order, forward time differencing.
- Upstream spatial differencing for both normal and tangential gradients.
- Phase speed computed at the current time.

The convexity property is satisfied in particular for tangential derivatives. The implicit time stepping escapes time-step restrictions by large phase speeds and small-scale noise, hence it allows a large time step without loss of stability (ROMS allows a substantial increase in the permissible time-step size; see Shchepetkin and McWilliams, 2000). It is also noteworthy that no additional array for storing boundary point values is necessary here; thus, the algorithmic implementation is simple.

The resulting scheme can be written as

$$\phi_{b,j}^{n+1} = \frac{1}{1+r_x} \left[ \phi_{b,j}^n + r_x \phi_{b-1,j}^{n+1} - r_y (\phi_{b,j}^n - \phi_{b,j-1}^n) \right] \quad \text{if } r_y > 0, \quad (4)$$

$$\phi_{b,j}^{n+1} = \frac{1}{1+r_x} \left[ \phi_{b,j}^n + r_x \phi_{b-1,j}^{n+1} - r_y (\phi_{b,j+1}^n - \phi_{b,j}^n) \right] \quad \text{if } r_y < 0 \quad (5)$$

with

$$r_x = - \frac{\Delta\phi_t \cdot \Delta\phi_x}{\Delta\phi_x^2 + \Delta\phi_y^2}, \quad (6)$$

$$r_y = - \frac{\Delta\phi_t \cdot \Delta\phi_y}{\Delta\phi_x^2 + \Delta\phi_y^2}, \quad (7)$$

$$\Delta\phi_t = \phi_{b-1,j}^{n+1} - \phi_{b-1,j}^n, \quad (8)$$

$$\Delta\phi_x = \phi_{b-1,j}^{n+1} - \phi_{b-2,j}^{n+1}, \quad (9)$$

$$\Delta\phi_y = \phi_{b-1,j}^n - \phi_{b-1,j-1}^n \quad \text{if } [\Delta\phi_t \times (\phi_{b-1,j+1}^n - \phi_{b-1,j-1}^n)] > 0, \quad (10)$$

$$\Delta\phi_y = \phi_{b-1,j+1}^n - \phi_{b-1,j}^n \quad \text{if } [\Delta\phi_t \times (\phi_{b-1,j+1}^n - \phi_{b-1,j-1}^n)] < 0, \quad (11)$$

where superscript  $n$  indicates the time, subscript  $b$  indicates the boundary normal position of the boundary point, and subscript  $j$  indicates the tangential position of the boundary point.

### 3.3. Implementation

The prognostic variables in a free-surface, Primitive-Equation model are surface elevation  $\eta$ ; barotropic horizontal velocity components  $(\bar{u}, \bar{v})$ ; baroclinic horizontal velocity components  $(u, v)$ ; and tracers such as temperature  $T$  and salinity  $S$  (additional tracers are added for biogeochemical simulations). Table 1 presents the standard implementation of our OBCs for each variable.

The radiation condition described above is used independently for all three-dimensional prognostic variables. There are two reasons. First, coupling at the boundary is made difficult by the position of the prognostic variables on a C-grid, as opposed to a B-grid. For example, it is not straightforward to compute at boundary points the baroclinic velocities from geostrophy as done in Stevens (1990). This point is discussed in more detail by Barnier et al. (1998) and Treguier et al. (2000). Second, the oblique radiation condition does not suffer from an instability generated by the interior advection terms and commonly observed when purely normal radiation conditions are applied to both velocity components independently (Raymond and Kuo, 1984; Palma and Matano, 1998).

The barotropic mode presents a different problem. In the open ocean, the external Rossby radius of deformation is over a 1000 km, which is greater than the horizontal scales in a regional oceanic domain. In both deep and shallow water, the horizontal scales of greatest interest are larger than the water depth. Therefore, non-dispersive (i.e. shallow water) surface gravity waves account for a large part of the transient barotropic signals calculated in a regional configuration. In a rigid-lid model the surface gravity waves are filtered and the barotropic mode has more of an elliptic nature, which may partly explain the good results obtained by simply specifying at the boundary the observational data (Treguier et al., 2000) or a Sverdrup solution (Stevens, 1990) for the barotropic flow. In a free-surface model, there needs to be a distinction between the different variables to handle well the surface gravity waves. Only the normal barotropic velocity

Table 1  
Implementation of the open boundary conditions

Variables	Passive regime	Active regime	Both
$u, v$	Oblique radiation Weak nudging	No radiation Strong nudging	Sponge layer
$T, S$	Oblique radiation Weak nudging	No radiation Strong nudging	Sponge and Nudging layers
$\bar{u}, \bar{v}$	Oblique radiation Weak nudging	No radiation Strong nudging	Sponge layer Volume constraint
$\eta$			Zero gradient

component at the boundary is used directly for the interior computation of these waves. The tangential component is used in the interior advection terms (which gets us back to the instability problem described above), but  $\eta$  is only used to estimate the interior water depth. Consequently, we used a zero-gradient condition at the boundary for this variable, and our oblique radiation scheme for both barotropic velocity components independently (Table 1).

Alternatively, for the normal component of barotropic velocity  $\bar{u}_n$ , we may consider the radiation condition proposed by Flather (1976) combining the Sommerfeld equation (with surface gravity waves phase speed) with a one-dimensional version of the continuity equation applied in the outwardly normal direction at an open boundary

$$\bar{u}_n = \bar{u}_n^{\text{ext}} - \sqrt{\frac{g}{h}}(\eta - \eta^{\text{ext}}), \quad (12)$$

where  $\bar{u}_n^{\text{ext}}$  represents the external data and  $h$  is the local water depth. In this equation, the differences between the external data and the model predictions are allowed to propagate out of the domain at the speed of the external gravity waves. The volume is automatically conserved in the domain and variations due to physical forcing such as tides (see Section 4.2) can be introduced through the external data. The propagation is always outward and does not require an adaptive scheme. This condition presents an interesting and inexpensive alternative for the barotropic mode to our extrapolation technique but is restricted to the physical assumption that surface gravity waves are dominant. This alternative condition is evaluated in Section 5.

### 3.4. Simple test problem

A simple test problem for the radiation condition is the propagation of a barotropic Rossby soliton on an equatorial beta-plane, for which an asymptotic solution exists to the inviscid, non-linear shallow water equations. The reader is referred to Haidvogel and Beckmann (1999) for a detailed description of a Rossby equatorial soliton experiment with ROMS. We reproduce a similar experiment here but use radiation instead of cyclic boundary conditions. In principle, the soliton should propagate westwards at fixed phase speed, without change of shape. Since the uniform propagation and shape preservation of the soliton are achieved through a delicate balance between linear wave dispersion and non-linear steepening, this is a difficult test for any OBC.

We test three cases:

1. normal radiation ( $c_y = 0$ ,  $\partial\phi/\partial y = 0$ ),
2. normal projection of oblique radiation (NPO;  $c_y = 0$ , but  $\partial\phi/\partial y \neq 0$ ), and
3. oblique radiation ( $c_y \neq 0$ ,  $\partial\phi/\partial y \neq 0$ ).

In the NPO case the normal phase speed is computed as the normal projection of the oblique phase speed, but the tangential phase speed is neglected. In the standard experiment (not shown), the Rossby soliton is initially positioned away from all four open boundaries. During an initial adjustment due to discrete approximations of the continuous solution, the soliton loses a small part of its initial amplitude. Then it propagates westward and reaches the western boundary with a normal phase speed. A general feature of OBCs is increased dispersion of outgoing signals which generate computational modes that can propagate inward and look like reflected waves. In all three cases, the soliton escapes the domain with only small reflection, although the NPO radiation produces the largest error. This may be attributed to the neglect of  $c_y$  which makes the radiation

scheme somewhat inconsistent. However, the test becomes more dramatic when the northern and southern boundaries are set on the edge of the soliton (Fig. 1). In this case, the zonal boundaries have to deal with tangential propagation. The results for the free surface are shown in Fig. 1. The soliton is partly reflected at the western boundary in all three cases, but there is a marked difference among them. The normal radiation method is worst since tangential propagation is

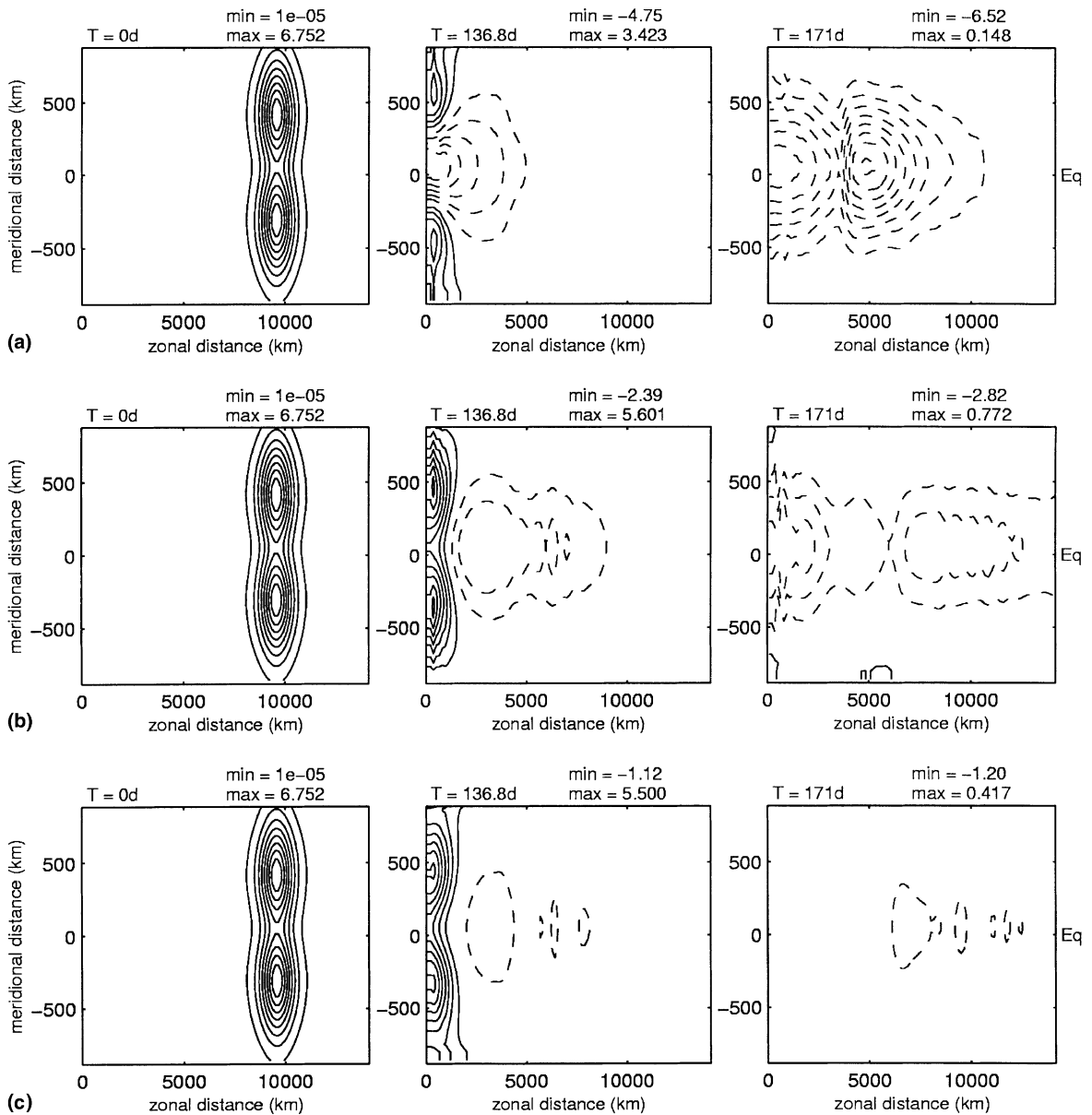


Fig. 1. Westward propagation of an equatorward Rossby soliton with four open boundaries. The radiation technique is (a) normal radiation, (b) normal projection of oblique radiation (NPO radiation), and (c) oblique radiation.

interpreted as normal propagation at the zonal boundaries. The soliton is absorbed from the sides, degrading in shape and amplitude, and finally reflecting badly at the western boundary. The oblique radiation method corrects significantly the problem allowing most of the package to propagate tangentially and then normally. The NPO radiation has intermediate results but is closer to the oblique case. When shortening the domain further meridionally, the situation changes again. Only the NPO radiation method is able to evacuate the soliton, while the two other cases lead to numerical blow up. The instability for the oblique case was previously noticed by Barnier et al. (1998), and the NPO radiation condition was eventually chosen for SPEM. In the present study we find this instability related to the persistency condition for inward propagation ( $c_x < 0$ ), although its exact cause is still obscure. The unstable behavior disappears when using adaptive control, that is when the persistency condition is removed. Therefore, we can choose for ROMS the oblique radiation condition for its superior radiation performances.

#### 4. Additional aspects of the boundary conditions

##### 4.1. Adaptivity

The adaptive technique is simple once there is a satisfactory estimate of the phase speed in the direction normal to the boundary. Miyakoda and Rosati (1977) suggested prescribing external data values when the computed normal phase speed is negative. However, large-scale information may be also needed during outward propagation because the PDE system is not completely hyperbolic. Even if we assume a well-posed mathematical problem and a radiation extrapolation with nil impedance, the model solution cannot be perfectly consistent with the external data. Therefore, if a boundary has outward propagation for some time, the predicted boundary values may have evolved to be quite different from the external data values. When the boundary propagation subsequently becomes inward, the sudden imposition of quite different boundary data may cause numerical difficulties. To overcome this problem, an additional nudging term is added to the radiation equation (1):

$$\frac{\partial \phi}{\partial t} + c_x \frac{\partial \phi}{\partial x} + c_y \frac{\partial \phi}{\partial y} = -\frac{1}{\tau}(\phi - \phi^{\text{ext}}) \quad (13)$$

with

$$\tau = \tau_{\text{out}} \quad \text{if } c_x > 0, \quad (14)$$

$$\tau = \tau_{\text{in}} \quad \text{and } c_x = c_y = 0 \quad \text{if } c_x < 0, \quad (15)$$

where  $\phi^{\text{ext}}$  represents the external data and  $\tau$  is the time scale for nudging, with  $\tau_{\text{out}} \gg \tau_{\text{in}}$ . During outward propagation, a weak nudging prevents substantial drifts while avoiding over-specification problems. During inward propagation, a strong nudging is applied but not so that it produces a data-shock problem. For the USWC circulation (Section 5), we find that the magnitude of  $\tau_{\text{out}}$  should be on the order of a year, while the magnitude of  $\tau_{\text{in}}$  should be a few days. Note that the meaning of the term *adaptivity* used in the present article differs from Penduff et al. (2000). The term refers here to the numerical algorithm rather than the physical solution.

#### 4.2. Volume constraint

Contrary to rigid-lid models, free-surface models may lose or gain water through the boundaries. In particular, the Sommerfeld equation does not respect volume conservation and may lead to a severe drift of mean sea level over long periods. Lack of volume conservation across open boundaries has been shown to introduce an accumulating dynamical error (Perkins et al., 1997). To prevent these problems, we add a volume constraint. The method consists of calculating the total volume transport through the open boundaries and uniformly adjusting the barotropic inflow at the open boundaries, so as to exactly balance the total volume transport. The time variation of total volume  $V$  in the regional domain is

$$\frac{dV}{dt} = \frac{d}{dt} \left[ \int \int \int_V dV \right] = \int \int_{S_b} \vec{u} \cdot \vec{n} dS = \int_{L_b} h \vec{u} \cdot \vec{n} dL, \quad (16)$$

where  $\vec{n}$  is the unit inward vector at the open boundary,  $S_b$  and  $L_b$  are, respectively, the total surface and total perimeter of the open boundary. We define a normal velocity correction  $\bar{u}_c$  to obtain the new barotropic solution,

$$\vec{u}_{\text{new}} = \vec{u} - \bar{u}_c \vec{n}, \quad (17)$$

such that the variation of total volume is only a result of physical sources and sinks of the sea-water ( $F$ ):

$$\frac{dV}{dt} = F = \int_{L_b} h \left( \vec{u} - \bar{u}_c \vec{n} \right) \cdot \vec{n} dL \quad (18)$$

$$= \int_{L_b} h \vec{u} \cdot \vec{n} dL - \int_{L_b} h \bar{u}_c dL. \quad (19)$$

Thus,  $\bar{u}_c$  is

$$\bar{u}_c = \frac{1}{S_b} \left( \int_{L_b} h \vec{u} \cdot \vec{n} dL - F \right). \quad (20)$$

In our USWC configuration we set  $F = 0$ , neglecting the effects of thermal expansion, evaporation, precipitation, river runoff, and tidal fluxes. The volume constraint, applied at every time step, only involves a small correction and does not appreciably affect the spatial structures in the flow since the same value is subtracted at every boundary point. An alternative to constraining lateral fluxes is to impose the mean sea level at open boundaries, as in Palma and Matano (2000). However, this method is often unstable since lateral fluxes tend to increase indefinitely (although Palma and Matano related their bad results to the use of radiation conditions rather than volume constraint).

#### 4.3. Sponge layers

The sponge layer is a region of increased horizontal viscosity near the open boundaries. Although the method might be considered inelegant, sponge layers have been shown to absorb disturbances and suppress computational noise associated with the radiation condition (Palma

and Matano, 1998), in particular for outgoing dispersive wave packets (Tang and Grimshaw, 1996). The sponge layer has been widely used in numerical weather forecasting because it can be a simple, efficient way to control over-specification problems. It has in particular the ability to restrict the region of error to the vicinity of the discontinuity (Oliger and Sundstrom, 1978). They are used in the USWC configuration for both momentum and tracer variables. Neumann conditions are used for higher-order boundary conditions related to friction terms.

#### 4.4. Nudging layers

The nudging layer is a region where a model data is relaxed towards external data. For this region a nudging term is added to the equations of tracers and surface elevation. Its mathematical form is added to the right-hand side of the prognostic equations as follows:

$$\frac{\partial \phi}{\partial t} = \text{r.h.s.} - \frac{1}{\tau} (\phi - \phi^{\text{ext}}). \quad (21)$$

Here  $\tau$  varies smoothly from  $\tau_{\text{out}}$  to infinity within about 100 km from the boundary in our USWC configuration. Consistent with the adaptive method, the nudging time-scale in the nudging layer is then always longer than it is at boundary points. Moderate nudging may prevent substantial drift, while overly strong nudging leads to over-specification (see Section 5).

## 5. Application

We have applied and tested the OBCs in a USWC configuration. A fuller description of the model configuration, solution properties, and comparisons with observation are in Marchesiello et al. (2000). Here we give only a brief summary.

### 5.1. Configuration

The domain extends in latitude from the middle of Baja California ( $\sim 28\text{N}$ ) to the Canadian border ( $\sim 48\text{N}$ ), approximately coincident with the subtropical/subpolar gyre boundary, and about 1000 km offshore, to encompass the California Current System (CCS) and its most energetic eddy variability. The surface forcing is by mean-seasonal wind stress, heat, and freshwater flux derived from COADS (da Silva et al., 1994), including thermal feedback (Barnier et al., 1995). Initialization is with Levitus and Boyer (1994) and Levitus et al. (1994)  $T$  and  $S$ , plus no flow. The model time step is 40 min, the horizontal mesh size is 5 km in the standard calculations, and the vertical grid has 20 levels with refinement approaching the upper surface.

There are three open boundaries at the western, northern, and southern borders. Often the flow and dominant waves are in opposite directions. Rossby waves transport a large amount of eddy kinetic energy to the west against the West Wind Drift, while Kelvin waves and other coastally trapped waves propagate northward against the California Current. Surface equatorward currents and the poleward undercurrent often flow in opposing directions across the open southern boundary. Therefore, because of the variety of mechanisms for information transfer through the open boundaries, the OBC problem is rather delicate in this region. Levitus et al.'s (1994)

mean-monthly  $T$ ,  $S$  and COADS winds are used to estimate climatological values for the geostrophic and Ekman baroclinic velocity components. A level of no motion at a depth of 500 m is assumed to determine the barotropic velocity. This climatology is used at open boundaries as the external data for all prognostic variables as described above. Values for  $(\tau_{in}, \tau_{out})$  are set to (1 day, 1 year) for the tracer and momentum fields. These are estimated from preliminary parameter studies as a successful compromise between over-specification and drift (for the present configuration). The model also uses the volume conservation, sponge, and nudging layers described previously. The values of the sponge and nudging parameters vary as a half-cosine function from a maximum at the boundary to zero at the inner edge of the layer; the layer width is set to 150 km (i.e. on the order of mesoscale structures); and the maximum viscosity/diffusivity values for the sponge layers are set to 100/50  $m^2 s^{-1}$ .

## 5.2. Results

Figure 2 depicts the time evolution of model kinetic energy (KE) at the surface and for the entire volume. After a spin-up period of about 2 years, the surface KE oscillates quasi-periodically around an equilibrium value, peaking in summer as observed with drifters and altimetry (Kelly et al., 1998). The volume-integrated KE does not show a clear seasonal cycle, though it does exhibit inter-annual variability as a consequence of the intrinsic variability due to mesoscale instabilities of the seasonally forced currents. The coherent evolution of the seasonal-mean flow is

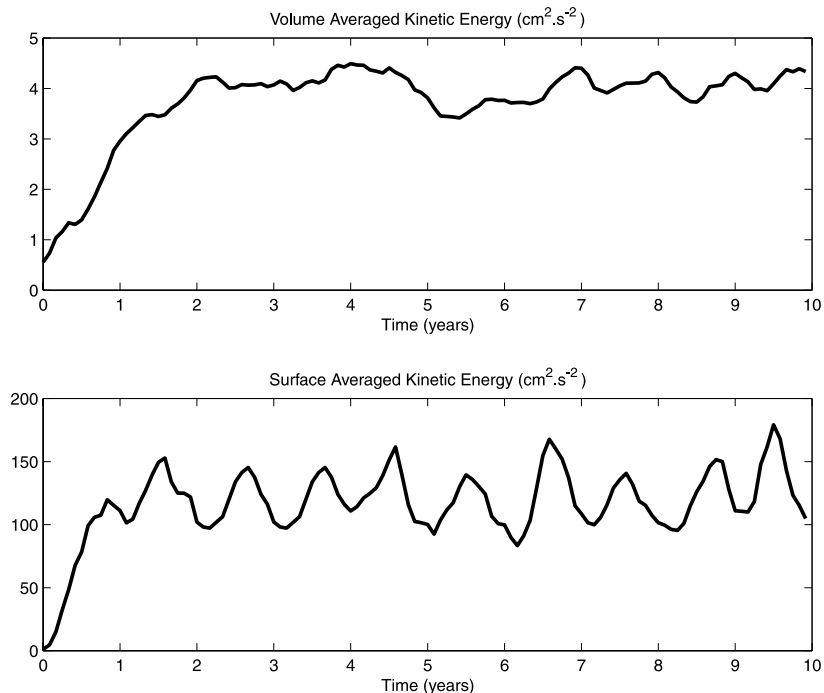


Fig. 2. Time evolution of the volume-averaged (top) and surface kinetic energy (bottom) in the USWC configuration at 5 km resolution.

conducted by the seasonal winds plus westward propagation at the rate of baroclinic Rossby waves. Figure 3 shows model-observation comparisons of summer mean surface elevation  $\bar{\eta}$  and surface eddy kinetic energy EKE, averaged over a period of 8 years. We chose the summer period for its peak energy levels caused by the strong long-shore winds through unstable coastal upwelling jets. It is also the best observed and documented season for the same reasons, which makes the comparisons more suitable. The observed  $\bar{\eta}$  field is derived from Boyer and Levitus (1997) annual climatology plus Levitus et al. (1994) summer component, assuming 500 m as level of no motion. The observed surface EKE is derived from a low-resolution interpolation of drifter data (Swenson and Niiler, 1996) mostly representative of summer season (P. Niiler, personal

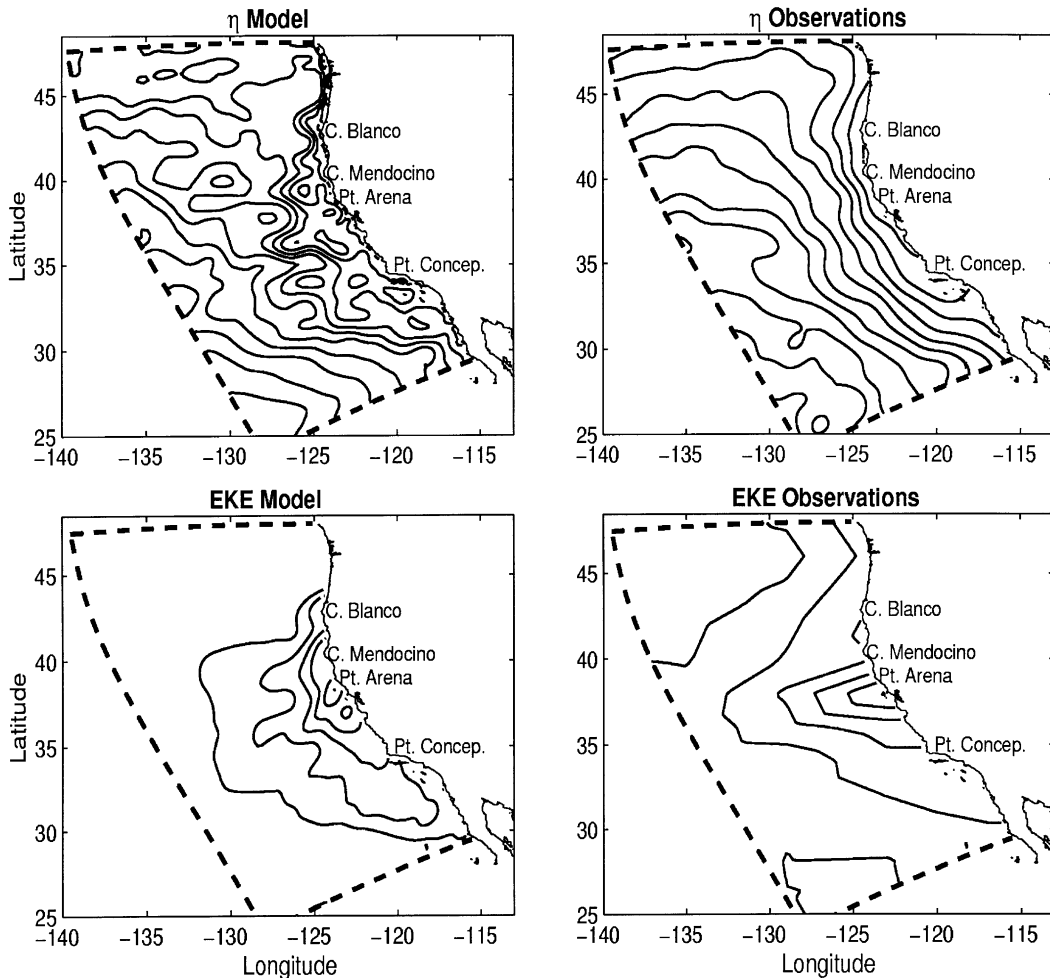


Fig. 3. Model-observation comparisons of summer-mean surface elevation  $\bar{\eta}$  and eddy kinetic energy EKE. The model data in (a) and (c) are averaged over a period of 8 years. The EKE in (c) is smoothed to allow for closer comparison with the observations. Plot (b) shows the dynamic height relative to 500 dB computed from Boyer and Levitus (1997) and (d) shows a smoothed climatology of the EKE from drifter arrays (Swenson and Niiler, 1996). The plotting parameters are for  $\eta$ : min = -25 cm, max = 25 cm, CI = 2 cm; for EKE: min = 0, max = 300 cm<sup>2</sup> s<sup>-2</sup>, CI = 50 cm<sup>2</sup> s<sup>-2</sup>.

communication). The surface mean and eddy fields are comparable in shape and magnitude with the observations. In particular, there is no evident mean or eddy energy trapped at the three open boundaries. The western inflow through the West Wind Drift and the southern outflow through the California Current maintain realistic shape and magnitude despite frequent upstream-propagating waves. The EKE has a triangular shape with maximum values south of Point Arena in both model and data. The peak magnitude is also about  $450 \text{ cm}^2 \text{ s}^{-2}$  in both cases.

## 6. Discussion

We conducted a sensitivity study for the OBC parameters in order to assess the performance of the algorithm and refine the choices. A less expensive, lower-resolution model (20 km) is used to allow multiple calculations, and, as a consequence, peak EKE values are about half as large as in the high-resolution run. We have seen that the model is stable without any damping at all (from the sponge layers). This can be attributed to the adaptive control and to proper respect of the convexity property in passive boundary conditions. However, a certain amount of damping is needed to suppress model–data inconsistencies in transitions between passive and active boundary conditions. We expect this problem to diminish as more compatible data are used from large-domain models that provide values of absolute velocity, rather than those estimated from an arbitrary level of no motion.

The radiation condition is robust. In our USWC configuration robustness is not a trivial matter as we learned from the wide range of conditions that we tried. In particular, we implemented reduced-physics equations as in Stevens (1990) without success (in the full three-dimensional configuration). It seems that the C-grid is not suitable for proper discretization of these equations (as discussed in Section 3.3). Likewise, different one-dimensional radiation conditions of the Orlanski type are unstable in the long term. The robustness in our OBCs appears to be related to the normal projection of the oblique phase speed as we compute the normal phase speed. The NPO radiation scheme ( $c_y = 0$ , but  $\partial\phi/\partial y \neq 0$ ) is robust even without adaptive control. Results with the NPO scheme are compared to the oblique radiation scheme in Fig. 4 (time evolution of KE), Fig. 5 ( $\bar{\eta}$ ), and Fig. 6 (EKE). They show that an equilibrium state is achieved in both cases. The EKE maps are similar, while  $\eta$  plots show a better control of inflows by the oblique radiation with less tangential error. We looked at a time series of phase speed  $c_x$  computed with the oblique radiation method for the different variables. It is confirmed that  $c_x$  has a clear physical meaning in case of high-amplitude perturbations (consistent with our assumption that  $c_x$  is slowly varying). However, high-frequency oscillations of  $c_x$  as reported by Treguier et al. (2000) are common for small amplitude perturbations, although there is no evidence in this case of significant reflection from the boundaries.

The use of radiation conditions alone without nudging to the external data is insufficient to maintain stability. As the OBCs are under-specified, the model solution drifts and eventually becomes numerically unstable after a few month. The adaptive nudging technique is successful in handling the external information. For comparison we present an experiment where the adaptive technique is suppressed, and the nudging layer has increased strength:  $\tau_{\text{out}} = 5$  days. This value is chosen to avoid significant drift of the interior solution and to be consistent with common practice of so-called *buffer-zones* (e.g. the Community Modeling Effort experiments, Bryan and Holland,

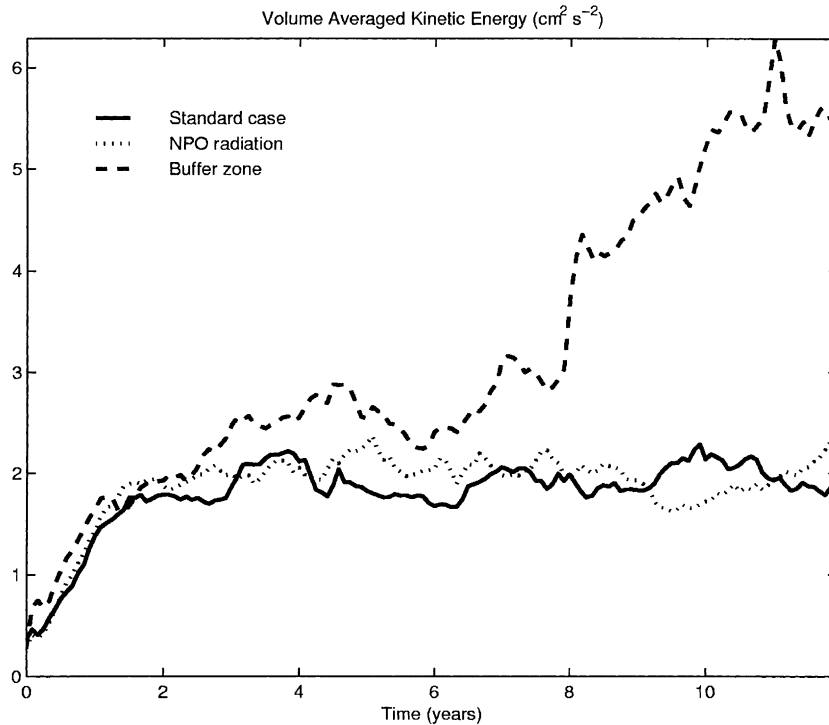


Fig. 4. Time evolution of the volume-averaged kinetic energy for the case of adaptive nudging with oblique radiation (solid line), adaptive nudging with NPO radiation (dotted line), and buffer zone with NPO radiation (dashed line).

1989). In Fig. 4 the model time evolutions are compared. Clearly, the buffer zone case fails to reach statistical equilibrium in spite of high-nudging parameters. The outward propagating energy is trapped at the western and southern boundaries as shown in Fig. 6(b); part is reflected to the interior domain (producing higher-coastal EKE). The west wind drift disappears (Fig. 5(b)) and is replaced by an artificial along-boundary current at the western side. This indicates an over-specification problem generated in nudging layers by dominantly outward propagation. In contrast, the adaptive approach allows an inflow of the West Wind Drift while eddy energy propagates outward with the Rossby waves.

We have shown that the radiation condition is robust and that adaptive nudging adequately incorporates the external information. The combination can be viewed as a nesting boundary condition that can better handle model–data inconsistencies than simply specifying data values at the boundary. Following Perkins et al. (1997) and Treguier et al. (2000), we conducted a test case with fixed boundary conditions to evaluate the performance of this approach to nesting. With fixed boundary conditions, because of the averaging used to discretize the equations, the flux across the open boundaries is still able to vary with time, resulting in lack of volume conservation if the latter is not constrained. In this case, the model surface elevation drifts and an accumulating dynamical error is introduced which results in the model blow up. On the other hand, the volume correction proved sufficient to stabilize the model. This result is consistent with the experiences of Perkins et al. (1997) and Treguier et al. (2000). In our USWC simulations, adding the volume correction

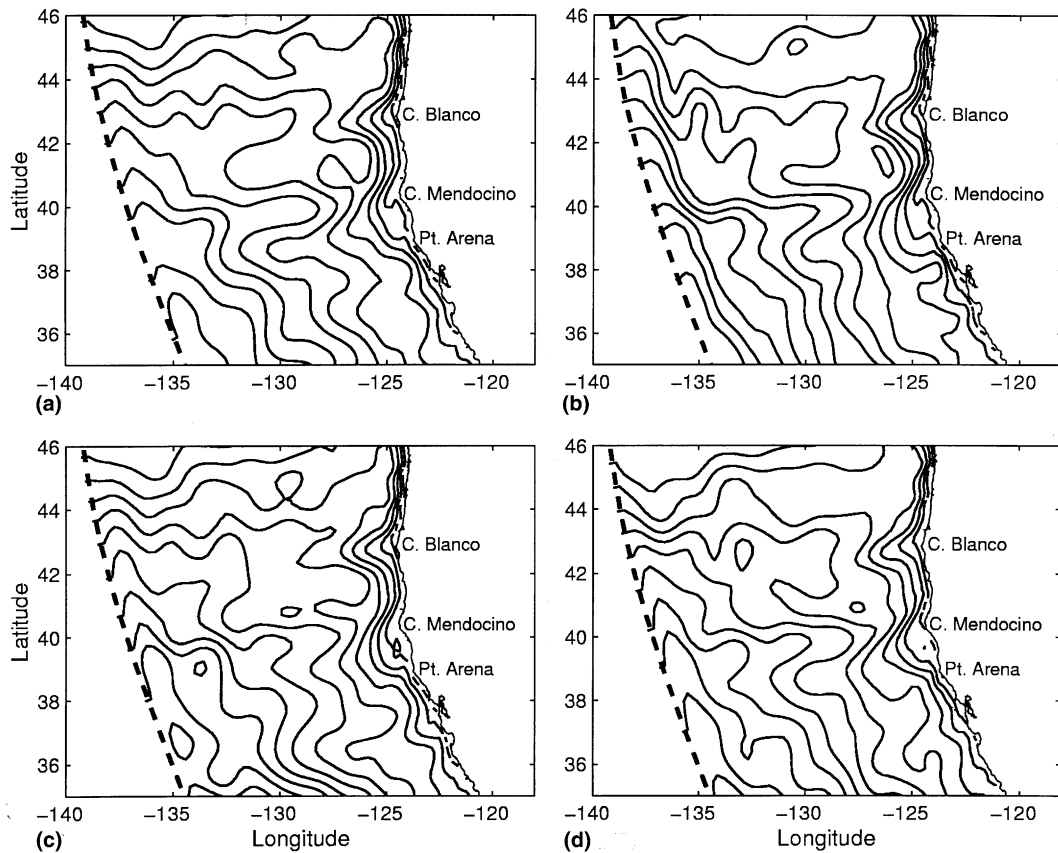


Fig. 5. Sensitivity of the USWC configuration (with 20 km resolution) to the boundary scheme: (a) adaptive nudging with oblique radiation (standard case), (b) buffer zone with NPO radiation, (c) adaptive nudging with NPO radiation, and (d) standard case but Flather's condition (1976) for the barotropic variables. All panels are 10-year averages of summer values for the surface elevation. Min = -25 cm, max = 25 cm, CI = 2 cm.

was an important step to improve the model stability and avoid accumulating errors on the long term. In the absence of radiation conditions, the sponge layer is able to dissipate a significant part of the energy accumulating near the boundary but does not eliminate the discontinuity resulting from model–data inconsistencies. The radiation condition on the other hand has numerical and physical means to reduce the discontinuity. Perkins et al. (1997) suggest that continuity at the open boundary is improved by radiating out model–data differences rather than absolute model values. This method is also implemented within our oblique radiation condition in the present USWC configuration. However, the results with smooth climatological data are similar to the standard case, and the performances will be rather evaluated in nesting problems. Following a similar idea, we also implemented the Flather (1976) condition for the barotropic mode, which had been recently recommended for the POM (Palma and Matano, 1998). The method is presented in Section 3.3 and results in Figs. 5(d) and 6(d). The condition leads to an over-specified problem as it generates a barotropic rim current at the western boundary (not shown), although the interior solution compares reasonably well with the standard case at the surface. Despite the

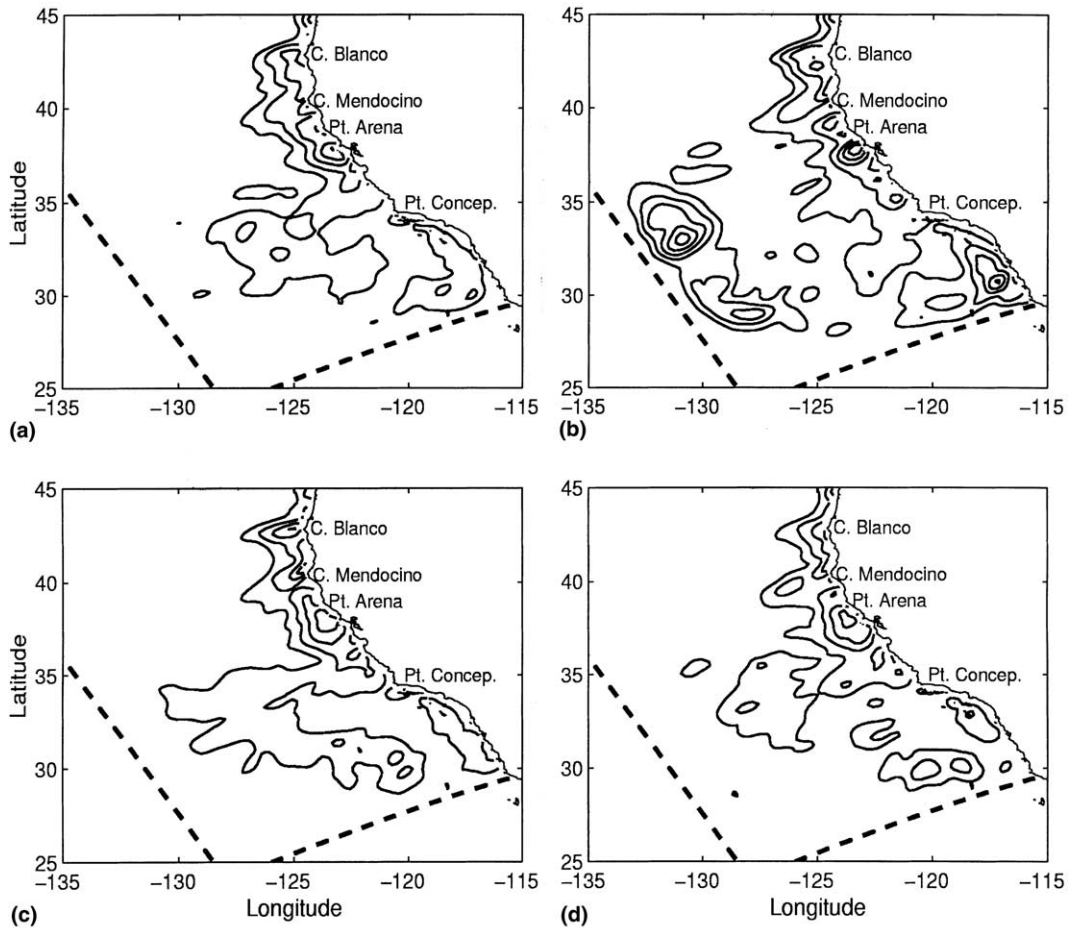


Fig. 6. Same as Fig. 5, but the comparison is made for the summer-mean eddy kinetic energy. Min = 0, max =  $200 \text{ cm}^2 \text{ s}^{-2}$ , CI =  $50 \text{ cm}^2 \text{ s}^{-2}$ .

inaccuracies of its radiation method, we retain from the Flather condition the idea of radiating model–data inconsistencies, the ability to enforce volume conservation, and the simplicity of its implementation. The Flather condition seems particularly suited to the treatment of tidal waves.

It is beyond the scope of this article to conduct an exhaustive study of the OBC problem. Experience shows that OBC performance can be configuration dependent, and we have as yet tested our OBC algorithm in only a limited number of configurations. However, the algorithm overcomes many of the known mathematical and numerical difficulties and allows us to study the dynamical equilibrium of a regional oceanic domain. This achievement is largely related to the proper estimation of the normal radiation phase speed which is used as precondition for an adaptive nudging to the external data and to enforced volume conservation. We are acquiring confidence in this OBC algorithm because other applications have shown similar success, while refining our choices. We need in particular to handle the influx of mesoscales and high-frequency

modes, such as tides or coastal waves prescribed either from observations or large-domain model solutions. This leads us towards grid nesting and the search for more comprehensive ways of modeling oceanic regions.

## Acknowledgements

This research has been supported by the Environmental Protection Agency (R825381), the National Science Foundation (OCE 96-33681), and the Office of Naval Research (N00014-00-1-0249). The support for computation was provided by the National Computational Science Alliance.

## References

- Barnier, B., Marchesiello, P., Pimenta de Miranda, A., Coulibaly, M., Molines, J.M., 1998. A sigma-coordinate primitive equation model for studying the circulation in the South Atlantic. Part I: model configuration with error estimates. *Deep Sea Research I* 45, 543–572.
- Barnier, B., Siefried, L., Marchesiello, P., 1995. Thermal forcing for a global ocean circulation model using a three-year climatology of ECMWF analyses. *Journal of Marine Systems* 6, 363–380.
- Bennett, A., 1992. *Inverse methods in physical oceanography*. Cambridge University Press, Cambridge, 346 pp.
- Blayo, E., Debreu, L., 1999. Adaptive mesh refinement for finite-difference ocean models: first experiments. *Journal of Physical Oceanography* 29, 1239–1249.
- Blumberg, A.F., Kantha, L.H., 1985. Open boundary conditions for circulation models. *Journal of Hydraulic Engineering* 11, 237–255.
- Boyer, T.P., Levitus, S., 1997. Objective analyses of temperature and salinity for the world ocean on a 1/4 degree grid. NOAA Atlas NESDIS 11, US Government Printing Office, Washington, DC, 62 pp.
- Bryan, F.O., Holland, W.R., 1989. A high resolution simulation of the wind- and thermohaline-driven circulation in the North Atlantic Ocean. In: Müller, P., Henderson, D. (Eds.), *Parametrization of Small Scale Processes: Aha Huliko'a Hawaiian Winter Workshop*. Hawaii Institute of Geophysics, Honolulu, pp. 99–115.
- Chapman, D.C., 1985. Numerical treatment of cross-shelf open boundaries in a barotropic coastal ocean model. *Journal of Physical Oceanography* 15, 1060–1075.
- Ezer, T., Ko, D.S., Mellor, G.L., 1992. Modeling and forecasting the Gulf Stream. *Marine Technology Society Journal* 26, 4–14.
- Flather, R.A., 1976. A tidal model of the northwest European continental shelf. *Memoires de la Societe Royale des Sciences de Liege* 6 (10), 141–164.
- Hetland, R.D., Signell, R.P., 2000. Numerical simulations of a river plume: a test case for ROMS. *Proceeding in the 2000 Ocean Sciences Meeting*.
- Haidvogel, D.B., Beckmann, A., 1999. *Numerical Ocean Modelling*, Imperial College Press, London, 330 pp.
- Kelly, K.A., Beardsley, R.C., Limeburner, R., Brink, K.H., Paduan, J.D., Chereskin, T.K., 1998. Variability of the near-surface eddy kinetic energy in the California Current based on altimetric drifter and moored current data. *Journal of Geophysical Research* 103, 13067–13083.
- Levitus, S., Boyer, T.P., 1994. *World Ocean Atlas 1994, vol. 4: Temperature*. NOAA Atlas NESDIS 4, US Government Printing Office, Washington, DC, 117 pp.
- Levitus, S., Burgett, R., Boyer, T.P., 1994. *World Ocean Atlas 1994, vol. 3: Salinity*. NOAA Atlas NESDIS 3, US Government Printing Office, Washington, DC, 99 pp.
- Marchesiello, P., Barnier, B., Pimenta de Miranda, A., 1998. A sigma-coordinate Primitive-Equation model for studying the circulation in the South Atlantic. Part II: meridional transports and seasonal variability. *Deep Sea Research I* 45, 573–608.

- Marchesiello, P., McWilliams, J.C., Shchepetkin, A., 2000. Seasonal cycle and intrinsic mesoscale variability of the California Current System. In preparation.
- Marchesiello, P., Middleton, J.H., 2000. Modeling the East Australian Current in the Western Tasman Sea. *Journal of Physical Oceanography* 30, 2956–2971.
- Matano, R.P., Philander, S.G.H., 1993. Heat and mass balances of the South Atlantic ocean calculated from a numerical model. *Journal of Geophysical Research* 98, 977–984.
- Miller, M.J., Thorpe, A.J., 1981. Radiation conditions for the lateral boundaries of limited-area numerical models. *Quarterly Journal of the Royal Meteorological Society* 107, 615–628.
- Miyakoda, A., Rosati, A., 1977. One way nested grid models: the interface condition and the numerical accuracy. *Monthly Weather Review* 105, 1092–1107.
- Oliger, J., Sundstrom, A., 1978. Theoretical and practical aspects of some initial boundary value problems in fluid dynamics. *SIAM Journal of Applied Mathematics* 35, 419–446.
- Orlanski, I., 1976. A simple boundary condition for unbounded hyperbolic flows. *Journal of Computational Physics* 21, 251–269.
- Palma, E.D., Matano, R.P., 1998. On the implementation of passive open boundary conditions for a general circulation model: the barotropic mode. *Journal of Geophysical Research* 103, 1319–1341.
- Palma, E.D., Matano, R.P., 2000. On the implementation of open boundary conditions for a general circulation model: the three-dimensional case. *Journal of Geophysical Research* 105, 8605–8628.
- Penduff, T., Barnier, B., Colin de Verdière, A., 2000. Self-adapting open boundaries for regional models: application to the Eastern North Atlantic. *Journal of Geophysical Research* 105, 11279–11297.
- Penven, P., Lutjeharms, J.R.E., Marchesiello, P., Roy, C., Weeks, S.J., 2000. Generation of cyclonic eddies by the Agulhas Current in the lee of the Agulhas Bank. *Geophysical Research Letters* 28, 1055–1058.
- Perkins, A.L., Smedstad, L.F., Blake, D.W., Heburn, G.W., Wallcraft, A.J., 1997. A new nested boundary condition for a Primitive-Equation ocean model. *Journal of Geophysical Research* 102, 3483–3500.
- Raymond, W.H., Kuo, H.L., 1984. A radiation boundary condition for multidimensional flows. *Quarterly Journal of the Royal Meteorological Society* 110, 535–551.
- Roed, L.P., Cooper, C., 1986. Open boundary conditions in numerical ocean models. In: O'Brien, J.J. (Ed.), *Advanced Physical Oceanographic Numerical Modeling*, NATO ASI Series C, vol. 186. pp. 411–436.
- Shchepetkin, A., McWilliams, J.C., 2000. Regional Ocean Model System: a split-explicit ocean model with a free-surface and topography-following vertical coordinate. In preparation.
- da Silva, A., Young, C., Levitus, S., 1994. *Atlas of Surface Marine Data 1994*, vols. 1–5. NOAA Atlas NESDIS 6–10, US Government Printing Office, Washington, DC.
- Sommerfeld, A., 1949. *Partial differential equations. Lecture Notes on Theoretical Physics*, vol. 6. Academic Press, San Diego, CA.
- Stevens, D.P., 1990. On open boundary conditions for three dimensional Primitive-Equation ocean circulation models. *Geophys. Astrophys. Fluid Dyn.* 51, 103–133.
- Stevens, D.P., 1991. The open boundary condition in the United Kingdom Fine-Resolution Antarctic Model. *Journal of Physical Oceanography* 21, 1494–1499.
- Swenson, M.S., Niiler, P.P., 1996. Statistical analysis of the surface circulation of the California Current. *Journal of Geophysical Research* 101, 22631–22645.
- Tang, Y., Grimshaw, R., 1996. Radiation boundary conditions in barotropic coastal ocean numerical models. *Journal of Computational Physics* 123, 96–110.
- Treguier, A.M., Barnier, B., de Miranda, A.P., Molines, J.M., Grima, N., Imbard, M., Madec, G., 2000. An Eddy Permitting model of the Atlantic circulation: evaluating open boundary conditions. *Journal of Geophysical Research*, submitted.